Provided for non-commercial research and educational use only.
Not for reproduction, distribution or commercial use.

This chapter was originally published in the book "Advances in Planar Lipid Bilayers and Liposomes," Vol. 12, published by Elsevier, and the attached copy is provided by Elsevier for the author's benefit and for the benefit of the author's institution, for non-commercial research and educational use including without limitation use in instruction at your institution, sending it to specific colleagues who know you, and providing a copy to your institution's administrator.

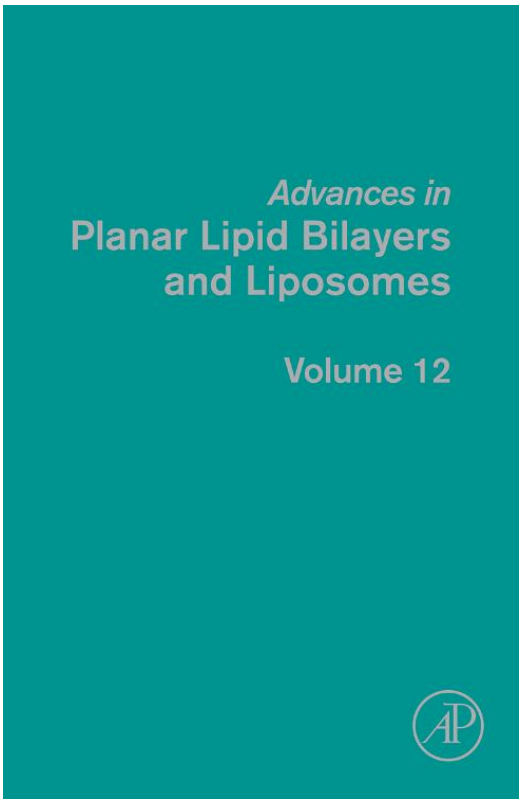

All other uses, reproduction and distribution, including without limitation commercial reprints, selling or licensing copies or access, or posting on open internet sites, your personal or institution's website or repository, are prohibited. For exceptions, permission may be sought for such use through Elsevier's permissions site at:
http://www.elsevier.com/locate/permissionusematerial

From: Norbert Kucˇerka, Mu-Ping Nieh, and John Katsaras, Small-Angle Scattering from Homogenous and Heterogeneous Lipid Bilayers,
In Dr. Alesˇ iglic and Dr. H.T. Tien editor:
"Advances in Planar Lipid Bilayers and Liposomes," Vol. 12.
Burlington: Academic Press, 2010, pp.201-236.
ISBN: 978-0-12-381266-7 © Copyright 2010,
Elsevier Inc. Academic Press.

Author's personal copy

CHAPTER EIGHT

Small-Angle Scattering from Homogenous and Heterogeneous Lipid Bilayers

Norbert Kučerka,[1,2,*] Mu-Ping Nieh,[1,3] *and* John Katsaras[1,4,5]

Contents

1. Introduction 202
2. Model-Independent Analysis 204
   2.1. The Guinier Plot 204
   2.2. Modified Guinier Plots 206
   2.3. The Porod Regime 206
   2.4. Interpretation of Slopes 206
   2.5. Applications to Lipid Aggregates 207
3. Scattering Form Factors for Homogeneous Bilayers 209
   3.1. The Use of Simple Bilayer Models in Neutron Scattering 210
   3.2. Asymmetric Bilayers 213
   3.3. Advanced Bilayer Models Used in X-ray Scattering 215
   3.4. Joint Refinement of Neutron and X-ray Scattering 217
   3.5. Lipid Area 221
4. Scattering from Laterally Heterogeneous ULVs 222
   4.1. Model-Independent Analysis 223
   4.2. Full Form Factor 226
   4.3. The Influence of Curvature on Domains 229
5. Concluding Remarks 231
References 231

* Corresponding author. Tel.: +613 584 8811 ext. 44195; Fax: +613 584 4040.
E-mail address: norbert.kucerka@nrc-cnrc.gc.ca

[1] Canadian Neutron Beam Centre, National Research Council, Chalk River, Ontario, Canada
[2] Department of Physical Chemistry of Drugs, Faculty of Pharmacy, Comenius University, Bratislava, Slovakia
[3] Institute of Materials Science/Department of Chemical, Materials & Biomolecular Engineering, University of Connecticut, Connecticut, USA
[4] Department of Physics, Brock University, St. Catharines, Ontario, Canada
[5] Guelph-Waterloo Physics Institute and Biophysics Interdepartmental Group, University of Guelph, Guelph, Ontario, Canada

Advances in Planar Lipid Bilayers and Liposomes, Volume 12 Crown Copyright © 2010. Published by Elsevier Inc.
ISSN 1554-4516, DOI: 10.1016/S1554-4516(10)12008-0 All rights reserved.

Author's personal copy

Abstract

Advances in colloid and interface science have stimulated a renewed interest in the study of lipid–water systems. At the same time, much progress has been made in regards to the analysis of small-angle X-ray and neutron scattering data. The popularity of small-angle scattering for the study of biologically relevant materials stems from the fact that it provides detailed information on the size, shape, and conformation of molecular assemblies in solution. Additionally, neutron scattering has the capability to accentuate, or nullify, the scattering from individual parts of a macromolecular complex with its unique ability to distinguish between hydrogen and its isotope deuterium. As a result, structural biophysics has taken advantage of recent developments in small-angle scattering to accurately determine the structure of lipid bilayers in both the transverse and lateral directions. An example is the joint refinement of X-ray and neutron scattering data, which has been used to improve the values of lipid areas that are commonly used in molecular dynamics simulations. Advances in neutron scattering theory have also made possible the determination of the membrane's in-plane organization by enabling the detection and characterization of nanoscopic domains.

1. Introduction

Biological membranes form the interface that encompass and define cells and biological tissue. Membranes form a natural hydrophobic barrier that contains cell contents, and also act as sites of contact for cell recognition and communication. The main objectives of biomembrane studies are molecular characterization, the determination of structure and interactions, and the evaluation of thermodynamic state and/or chemical composition changes in the molecular components that make up membranes. Careful examination of the above results in the appropriate modeling of a biological membrane. One of the most popular models used to describe the structure of a biological membrane is the fluid mosaic model [1], which is composed of a phospholipid bilayer matrix with membrane associated and peripheral proteins. Although the basic notion of the fluid mosaic model still holds true, the plasma membrane has since been shown to be considerably more complex, especially with regard to the diversity and function of lipids [2]. An example is lipid rafts, regions of membranes enriched in certain types of lipids and cholesterol, and which are thought to act as functionalized platforms. Thus, besides proteins playing an active role in carrying out the various functions that take place in a biological membrane, much attention has recently focused on the importance of lipids in membrane function. After all, how better to explain the diversity of lipids found in nature?

Author's personal copy

There are a number of experimental techniques that are suitable for the study of self-assembled lipid dispersions at the microscopic level. For example, microscopic techniques provide direct information on phases and local structures ranging from the micron to the nanometer length scale. On the other hand, samples that need to be studied *in situ* under biologically relevant conditions can be investigated, for the most part, at the expense of spatial resolution (e.g., various optical microscopies), or by probing the sample's surface (e.g., AFM—atomic force microscopy) [3]. In contrast, scattering techniques allow for the *in situ* manipulation of samples while providing quantitative data on the global distribution of structural features, size, shape, and correlation lengths. Among the often used spectrometric techniques (e.g., EPR—electron paramagnetic resonance, NMR—nuclear magnetic resonance, fluorescence) and calorimetry, the scattering of X-rays and neutrons is probably the most important and widely utilized experimental approach employed for the study of biological membranes [4]. Well known are the advances in atomic resolution X-ray crystallography, especially for the determination of protein crystal structures. However, scattering methods have much wider use in polymer research, colloid chemistry, and materials studies. In addition, the various neutron and X-ray scattering techniques often complement crystallographic studies that require hard-to-obtain high quality crystals of macromolecules. Perhaps even more importantly, small-angle neutron scattering (SANS) and small-angle X-ray scattering (SAXS) are structural techniques capable of studying biomolecules in solution under biologically relevant conditions.

Neutron and X-ray scattering are similar in that both techniques are capable of providing dynamical and structural information [5]. However, the principal differences between the two techniques are in their interactions with matter. As X-rays are electromagnetic waves that primarily interact with electrons, the amplitude of X-ray scattering increases in a simple way with atomic number. On the other hand, neutrons are elementary particles that interact with atomic nuclei, and neutron scattering amplitudes depend in a complex manner on the mass, spin, and energy levels of nuclei. Additionally, differences in the interaction of neutrons with the various isotopes of the same element allow for the powerful and commonly used method of contrast variation. This technique, in which hydrogen atoms that are ubiquitous in biologically relevant samples are substituted with deuterium atoms, is commonly used in neutron scattering studies.

In a scattering experiment a planar wave with a well-defined direction of incidence $\overrightarrow{k_0}$ interacts with the object's electron, or nucleus, that itself becomes a source of spherical waves [6]. The experimentally observed scattered intensity then describes the constructive interference between the waves scattered by atoms as a function of angle, defined by $\overrightarrow{k}$. Defining the scattering vector as a change in the momentum transfer ($\overrightarrow{q} = \overrightarrow{k} - \overrightarrow{k_0}$) then

Author's personal copy

maps out all scattering into reciprocal space. The magnitude of $\vec{q}$ is simply $|\vec{q}| = 4\pi/\lambda \sin(\theta/2)$, where λ and θ are the wavelength of the incident wave and the scattering angle, respectively. Finally, the ability of the atom to scatter is expressed in terms of a scattering length (corresponding to the neutron scattering length in the case of neutrons or the number of electrons in the case of X-ray scattering) or a density function $\rho(\vec{r})$ in the case of continuous objects, which then allows us to express scattering form factors on the basis of the Born approximation as

$$F(\vec{q}) = 4\pi \int \rho(\vec{r}) \exp(i\vec{q} \cdot \vec{r}) \mathrm{d}\vec{r}, \tag{1}$$

where the scattered intensity is simply expressed as $I(\vec{q}) = |F(\vec{q})|^2$. Further assumptions can then be applied to simplify the interpretation of small-angle scattering data, of which some of the most important examples will be discussed in this chapter.

2. Model-Independent Analysis

Amphiphilic molecules (e.g., lipids, surfactants, etc.) can self-assemble into a variety of aggregates in aqueous solutions. Some of them form structures with three well-defined dimensions having length scales on the order of nanometers (e.g., spherical micelles, unilamellar vesicles—ULVs), while others may only have one and/or two well-defined dimensions (e.g., the thickness of lamellae and the cross-section of cylindrical micelles). For the most part, SANS and SAXS turn out to be the most effective tools for identifying the global aggregate morphologies of amphiphilic molecules. Generally speaking there are two approaches to analyzing SANS and SAXS data i.e., model independent and model dependent. The former is usually applied in cases where the gross morphology needs to be identified along with characteristic length scales. The modeling method, on the other hand, can yield detailed structural information. In this section, we will discuss various model independent approaches commonly reported in the literature; however, cases where the interparticle interaction (structure factor) is required will not be addressed.

2.1. The Guinier Plot

Here we introduce a structural parameter that is closely associated with the small-angle scattering method, namely that of the root mean square radius of gyration, $\langle {R_G}^2 \rangle^{1/2}$, which is defined as $\left\langle \sum_{i=1}^{n} m_i x_i^2 / \sum_{i=1}^{n} m_i \right\rangle^{1/2}$, where m_i

Author's personal copy

and x_i are the mass of component i and its distance to the center of the mass of the aggregate, respectively (Fig. 1). Thus $\langle R_G{}^2\rangle^{1/2}$ can be calculated for different morphologies (Table 1). For any aggregate with $\langle R_G{}^2\rangle^{1/2} \ll 1/\ q$, the scattering intensity $I(q)$ can be approximated as [7]

$$\log(I(q)) = \log(I_0) - q^2\frac{\langle R_G^2\rangle}{3} + \cdots, \tag{2}$$

where I_0 is the extrapolated zero angle intensity. Therefore, a straight line is expected in the case where $I(q)$ is plotted with q^2, the slope of which is $-\langle R_G{}^2\rangle/3$. This is commonly known as a Guinier plot. It should be noted that the obtained $\langle R_G{}^2\rangle^{1/2}$ is independent of the aggregate morphology.

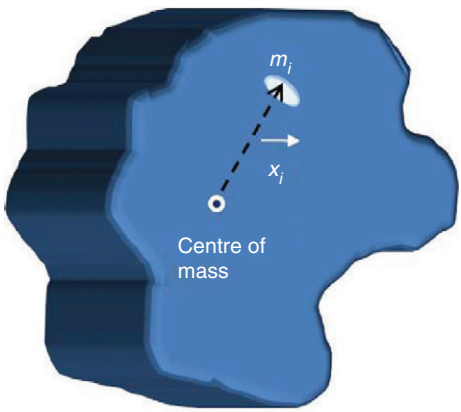

Figure 1 The component i has a mass of m_i and a distance of x_i from the center of mass. $\langle R_G{}^2\rangle^{1/2}$ is defined as $\left\langle \sum_{i=1}^{n} m_i x_i^2 / \sum_{i=1}^{n} m_i \right\rangle^{1/2}$.

Table 1 Calculated $\langle R_G{}^2\rangle^{1/2}$ for various morphologies

Objects	$\langle R_G{}^2\rangle^{1/2}$
Sphere with a radius R	$\sqrt{\frac{3}{5}}R$
Spherical shell with an outer and inner radius of R_o and R_i, respectively	$\sqrt{\frac{3\left(R_o^5-R_i^5\right)}{5\left(R_o^3-R_i^3\right)}}$
Cylinder with a radius R and a length t; therefore:	$\sqrt{\frac{R^2}{2}+\frac{t^2}{12}}$
Long rod: $R \to 0$ and t≫R	$\frac{t}{\sqrt{12}}$
Thin disk: $t \to 0$ and R≫t	$\frac{R}{\sqrt{2}}$

Author's personal copy

2.2. Modified Guinier Plots

The concept of a Guinier plot can be further applied to 2D (e.g., lamellae) or 1D (e.g., long cylinders) objects. In the case of extended cylinders of length L and radius R_{cyl}, where $R_{\mathrm{cyl}} \ll 1/\ q \ll L$, the Guinier plot can be written as [8]

$$\log(q \cdot I(q)) = A - q^2 \frac{\left\langle R_{\mathrm{G,cyl}}^2 \right\rangle}{2} + \cdots, \tag{3}$$

where A is the extrapolated intercept value at the $\log(q \cdot I)$ axis and $\langle R_{\mathrm{cyl}}{}^2 \rangle^{1/2}$ is the root mean square radius of gyration of the cylinder's cross-section ($= R_{\mathrm{cyl}}/\sqrt{2}$). A similar approach can be applied to the study of large lamellar structures of thickness t, where $t \ll 1/q \ll$ than the lateral dimensions of the lamellae

$$\log\left(q^2 \cdot I(q)\right) = B - q^2 \left\langle R_{\mathrm{G,t}}^2 \right\rangle + \cdots, \tag{4}$$

where B is the extrapolated intercept value at the $\log(q^2 \cdot I)$ axis and $\langle R_{\mathrm{G},t}{}^2 \rangle^{1/2}$ is the root mean square radius of gyration of the lamellar thickness ($= t/\sqrt{12}$). Although a modified Guinier plot is powerful in probing a morphology's average dimensions, it should be stressed that a uniform scattering density profile (SDP) is assumed and the precise morphology of the aggregates is not determined.

2.3. The Porod Regime

In contrast to the Guinier regime where the q range of interest is less than the reciprocal dimension of the object, the Porod regime is defined as $q \gg 1/$(the smallest dimension). In this high q regime of scattering, the scattered intensity is mainly the result of scattering from the interface between the aggregates and the solvent, and can be approximated as [9]

$$q^4 \cdot I(q) = 2\pi \Delta\rho^2 S_{\mathrm{T}}, \tag{5}$$

where $\Delta\rho^2$ and S_{T} are the contrast factor and the total surface area of the aggregates per unit volume. Equation (5) also indicates that $\log(I)$ decreases linearly when plotted against $\log(q)$, with a slope of -4 in the Porod regime.

2.4. Interpretation of Slopes

In the case of monotonic decay data (both SANS and SAXS), there is another commonly used method to identify morphologies, namely determining the slope of a $\log(I)$ vs $\log(q)$ plot (i.e., $I \sim q^{-m}$). The value of m

Author's personal copy

reveals the system's overall structure, where $m = 1, 2, 3$, and ~ 4 represents cylinders, lamellae (disks), 3D fractal objects, and sharp interfaces (Porod's law), respectively [10]. Generally speaking, the q interval of one slope should span at least a decade in reciprocal space in order to be confident that the assumed morphology has been correctly identified. The dimension of interest can also be estimated by the q value, $q_{\min}$, where the transition of the slope takes place. Figure 2 shows simulated scattering data of cylinders (solid curve) and disks (dashed curve), where the length of the cylinders and the diameter of the disks can be estimated to be $\sim \pi / q_{\min}$.

2.5. Applications to Lipid Aggregates

Model independent analysis is robust in determining the gross morphologies of interest as well as providing the foundation for more sophisticated models needed to obtain detailed structural information. For the most part, liposomes can be classified into two main catagories: (a) ULVs whose sizes span range from small unilamellar vesicles (SUVs) to giant unilamellar vesicles (GUVs), and (b) multilamellar vesicles (MLVs), which can easily be distinguished by SANS and SAXS (as shown in Fig. 3). MLVs are commonly observed in long-chain zwitterionic lipid aqueous solutions, where hydration reaches a maximum as a result of the balance between van der Waals, undulation, and Coulombic forces, yielding a regular lamellar spacing

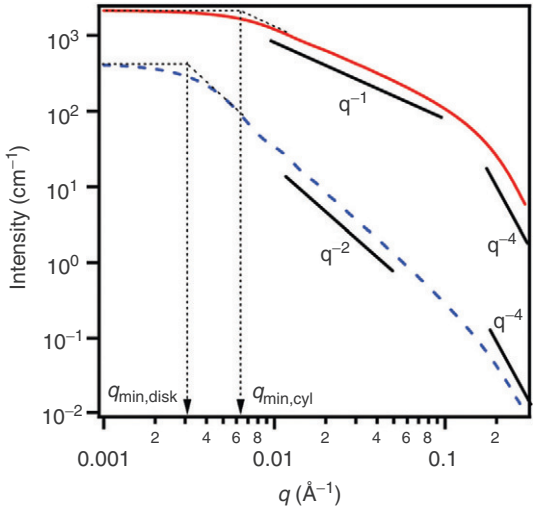

Figure 2 The calculated scattering curves of long cylinders (solid curve) and large disks (dashed curves), where the length of the cylinders and the diameter of the disk cross-section are 500 and 1000 Å, respectively, $\sim \pi / q_{\min}$.

Author's personal copy

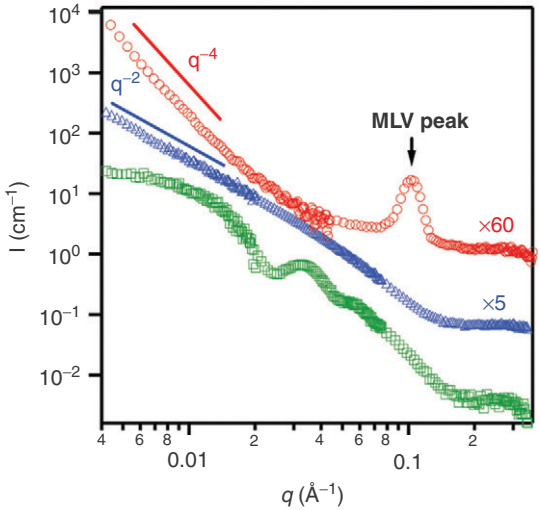

Figure 3 SANS data of 0.1 wt% phospholipid solutions prepared by different methods illustrating the three distinct curves resulting from: MLVs (circles), micron size ULVs (triangles), and low-polydispersity submicron ULVs (squares).

characteristic to a given lipid. This structure then gives rise to a set of discrete quasi-Bragg peaks. Moreover, because of their micrometer size, the Guinier regime for these samples is normally not accessible by SANS or SAXS. In most cases, the decay of $I(q)$ in the Porod regime falls in-between a q^{-2} (lamellae) and a q^{-4} behavior at high q values, depending on the lamellar spacing of the sample [11,12].

Micrometer size ULVs can be found in a number of zwitterionic lipid preparations [13–15] or charged lipid solutions [16,17]. The SANS or SAXS curve exhibits an initial q^{-2} dependence (because of the lamellar structure), followed by a q^{-4} monotonic decay (Fig. 3), where the location of the transient slope depends on the bilayer thickness. Submicron ULVs do not naturally form in single-component lipid/surfactant aqueous solutions, but are formed by mechanical processes whereby MLV solutions are sonicated or extruded. However, spontaneously formed ULVs of various sizes have been found to form in cationic/anionic surfactant mixtures [18–20] and long-chain/short-chain lipid mixtures [21–23]. In some cases, dilution, change in pH, or an extreme change in temperature can trigger the formation of ULVs [24–26]. The characteristic SANS or SAXS ULV curves (on a log–log plot) of usually contain a seemingly plateau region at low q, followed by a series of oscillations which sit on a curve with a q^{-2} (medium q) and q^{-4} decay (high q), as shown in Fig. 3.

Author's personal copy

After the initial evaluation of aggregate morphologies, the use of a model enables the determination of more detailed information regarding the average size, polydispersity, and bilayer thickness. The use of appropriate models to fit data will be discussed later on.

3. Scattering Form Factors for Homogeneous Bilayers

The thickness of biological membranes is known to vary, most likely to stimulate the functions associated with the various membrane proteins. For example, it is known that the activity of integral membrane proteins, as well as the insertion and orientation of polypeptides, critically depends, among other things, on bilayer thickness [27]. On the other hand, because of the structural flexibility exhibited by lipid hydrocarbon chains, a membrane can adjust its thickness in order to minimize unfavorable thermodynamic interactions between water and hydrophobic protein surfaces, a process commonly known as hydrophobic matching [28]. An example of this is sarcoplasmic reticulum Ca^{2+}-transporting ATPase reconstituted into bilayers made up of monounsaturated phospholipids and a biological detergent [29]. In this case, enzymatic activity is maximal in bilayers composed of medium length (18 carbons) lipids, and decreases as much as four times, in both short- (14 carbons) and long-chain (22 carbons) lipid bilayers. It is thus evident that knowledge of bilayer thickness is very important when it comes to understanding protein–bilayer interactions in membranes.

From a biological perspective, bilayers of ULVs are most appealing mimics of biological membranes. Two of the simplest and common methods used to determine the bilayer thickness of ULVs are SAXS and SANS. In the case of SANS, bilayer thickness can be obtained from Guinier/Porod plots in the limited q range (see Section 2), or by fitting the scattering function over a broader range of scattering vectors using a suitable model for the ULV. In both cases, typical lipid bilayers dispersed in D_2O (often used instead of H_2O to increase scattering contrast in neutron experiments) can be modeled using simple slab profiles [30]. On the other hand, as a result of selective deuteration, SANS also allows for the positional determination of phospholipid groups and/or water [31].

An alternative way of obtaining bilayer thickness is from the Bragg scattering associated with high resolution data (i.e., extended q range), especially in the case of X-ray scattering, where data can be obtained at higher q values. For example, from such data the resultant 1D electron density (ED) profile contains information regarding the position of the electron rich phosphate groups

Author's personal copy

that are associated with the phosphatidylcholine headgroup. The headgroup peak-to-peak distance across the bilayer is then used to calculate the bilayers thickness [32]. However, bilayer thicknesses from X-ray scattering data have come under closer scrutiny as of late, namely by a technique that jointly refines X-ray and neutron scattering simultaneously [33].

3.1. The Use of Simple Bilayer Models in Neutron Scattering

SANS data are most often evaluated using an oversimplified single-slab model ("top-hat") which describes the neutron scattering length density (NSLD) with a constant function. Although this model can reliably capture the relative changes to the bilayer's overall thickness, it neglects its internal structural details. At a minimum, a lipid bilayer consists of three distinct slabs, one for the hydrocarbon region and two for the polar headgroups, which also include water molecules. Although still simple, the three-slab model is a more realistic representation of the lipid bilayer [34].

In the case of the three-slab model, although the central slab is well approximated by a constant function, the interface between the lipid headgroup region and water region is better described by a smooth function. For example, models employed in analyzing high resolution reflectometry data often utilize classical error functions to describe broad interfaces [35]. However, the calculation of scattered intensity is not trivial in the case of such complex models. In addition, the amplitude of scattered intensity from ULVs decays as the square of the scattering vector q. A typical measurement can then detect the scattered intensity above the background scattering only in the range of $q < 0.2\ \text{Å}^{-1}$, and does not provide the necessary resolution to resolve detailed bilayer features.

An important consideration when analyzing small-angle scattering data from ULVs is their polydispersity. The distribution of their sizes (i.e., radii R) follows a statistical function that is best represented either by a Gaussian [36] or a Schulz distribution function [37]. Both of these functions have a similar general form, with the Gaussian function being symmetric in shape. On the other hand, polydisperse ULV systems are better described by the asymmetric Schulz distribution

$$f(R) = \left(\frac{t+1}{R_{\text{mean}}}\right)^{t+1} \frac{R^t}{\Gamma(t+1)} \exp\left[-\frac{t+1}{R_{\text{mean}}} r\right]; \quad t = \left(\frac{R_{\text{mean}}}{\sigma}\right)^2 - 1, \quad (6)$$

where R_{mean} is a mean radius and σ represents the variance of ULV radii from which polydispersity is expressed in terms of a relative variance (σ/R_{mean}). The calculated intensity scattered from a single ULV is then

Author's personal copy

convoluted with the polydispersity distribution function in order to obtain the total intensity scattered from the entire system of ULVs as

$$I(q) = \int f(R) I(q, R)\, \mathrm{d}R, \tag{7}$$

and where the scattered intensity from a single ULV can be written in a Rayleigh–Gans–Debye form [38] as follows:

$$I(q, R) = \left[\int_{R-d/2}^{R+d/2} 4\pi r^2 (\rho(r) - \rho_{\mathrm{W}}) \frac{\sin(qr)}{qr} \mathrm{d}r \right]^2. \tag{8}$$

In general, the analytical solution of Eq. (7) is not possible in an exact form, and even numerical solutions are limited to simple models of NSLD profiles (e.g., step functions). On the other hand, it is possible to separate the bilayer and vesicle form factors when the bilayer thickness, d, is much less than the ULV radius R (i.e., $R + d \approx R$), and holds true for most cases. This then results in the separated form factors (SFF) approximation [39], where the total intensity is calculated as the product of two integrals instead of the convoluted integral given above. An advantage of the SFF calculation is that much more complex functions can be utilized in modeling the NSLD profile across the lipid bilayer.

Further simplification of Eq. (7) is achieved by the application of the Laplace transform method to the SFF approximation for Schulz-distributed ULVs [40]. The analytical form of total scattering intensity consists of the Fourier transform of the water subtracted bilayer NSLD profile (i.e., $\Delta\rho(z) = \rho(z) - \rho_{\mathrm{W}}$) and the function that includes the ULV's "sphericity" and polydispersity

$$I(q) = \left[\int_{-d/2}^{d/2} \Delta\rho(z) \cos(qz) \mathrm{d}z \right]^2 \times \frac{8\pi^2 (t+1)(t+2)}{s^2 q^2} \left\{ 1 - \left(1 + \frac{4q^2}{s^2} \right)^{-(t+3)/2} \cos[(t+3) \arctan(2q/s)] \right\}. \tag{9}$$

Compared to the numerical computation typically used in Eq. (7), the analytic form (Eq. (9)) allows for the much faster computation of the scattered intensity. More importantly, a simple integration of the first part enables one to express $\Delta\rho(z)$ in terms of much more complex functions than those already discussed. Figure 4 shows an example in which the bilayer NSLD profile is described by the single-slab model and where the bilayer–water interface is described by an error function

Author's personal copy

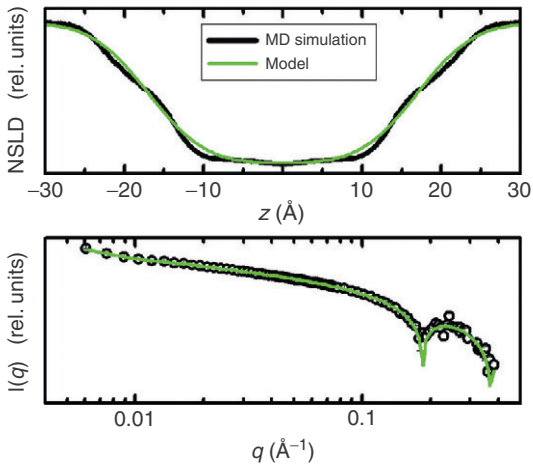

Figure 4 A single-slab step model of a lipid bilayer, where the bilayer–water interface is described by an error function. The top panel compares the neutron scattering length density (NSLD) profile obtained from fitting a model to molecular dynamics (MD) generated data (bottom panel) [34]. The bottom panel shows the MD generated data and the fit to the reciprocal space data using a model.

$$\Delta\rho(z) = \frac{\rho_{\mathrm{B}} - \rho_{\mathrm{W}}}{2}\left(\mathrm{erf}\left(\frac{z + z_i}{\sqrt{2}\sigma_i}\right) - \mathrm{erf}\left(\frac{z - z_i}{\sqrt{2}\sigma_i}\right)\right), \tag{10}$$

where ρ_{W} and ρ_{B} are NSLDs of the water and the bilayer respectively, and z_i and σ_i correspond to the central position and width of the interface. The first part of the scattered intensity (Eq. (9)) that corresponds to the scattering from a single bilayer is then expressed as

$$I_{\mathrm{B}}(q) = \left[\frac{2}{q}(\rho_{\mathrm{B}} - \rho_{\mathrm{W}})\left(\sin(qz_i)\exp\left(-\frac{(q\sigma_i)^2}{2}\right)\right)\right]^2. \tag{11}$$

This approach can be further expanded through the use of several error functions, as has been recently proposed for the analysis of high resolution neutron reflectometry data (Frank Heinrich, personal communication).

The scattered intensity falls on a curve that features two regimes corresponding to two different length scales. In the case of low-polydispersity ULVs, high frequency oscillations are observed at length scales corresponding to $q < 0.03$ Å^{-1}. These oscillations originate from scattering taking place over the entire vesicle and are inversely proportional to the ULV's radius, R, as can be surmised from the second part of Eq. (9). However, this feature decays quickly with increasing q [33]. Scattering

Author's personal copy

information from $q > 0.03$ Å^{-1} is mostly attributed to the bilayer itself. According to the relation between real space and reciprocal space ($D = 2\pi/q$), it is evident that detailed bilayer information can be extracted from high q data. Nevertheless, because the main feature of the NSLD is the contrast between water and the lipid, neutron scattering is a well-suited technique at describing a lipid bilayer's gross morphology, where by the time the scattered intensity reaches values of $q \sim 0.2$–0.3 Å^{-1}, it becomes indistinguishable from the background.

The situation is very different in the case of X-ray scattering, the result of the interaction between X-rays and the bilayer's electrons. A typical bilayer ED profile contains two distinct peaks corresponding to the electron-dense phosphate groups and the terminal methyl groups found in the bilayer's center. Consequently, it is often possible to obtain meaningful data up to $q = 0.6$ Å^{-1} in the case of unoriented ULV samples [41], and up to $q = 0.8$ Å^{-1} in the case of oriented multilayers [42]. In other words, X-ray scattering is well-suited at determining the bilayer's finer structural details.

3.2. Asymmetric Bilayers

Equation (11) was derived via the well-known Fourier transform for a symmetric (i.e., two identical bilayers leaflets) lipid bilayer NSLD profile (see Fig. 4). Its behavior for a typical lipid bilayer is characterized by periodic oscillations that have zero intensity at certain points along q. On the other hand, a nonzero intensity along q suggests bilayer asymmetry, as can be surmised from the complete form (Eq. (12)) of the Fourier transform with a complex exponential

$$I_B(q) = \left[\int_{-d/2}^{d/2} \Delta\rho(z)\cos(qz)\,dz\right]^2 + \left[\int_{-d/2}^{d/2} \Delta\rho(z)\sin(qz)\,dz\right]^2. \quad (12)$$

For an asymmetric lipid bilayer the amplitude of scattered intensity does not necessarily go to zero (see Fig. 5), as was observed in SAXS experiments of charged lipid bilayers [41,43].

Whereas aligned bilayers, whether prepared with charged or uncharged lipids, are symmetric, experimental results have shown this not necessarily the case in ULVs of charged lipids—it should be pointed out, however, that similarly sized neutral ULV bilayers are not affected by curvature. These data implied that the asymmetry observed in charged bilayers is most likely the result of the interplay between electrostatic interactions and curvature, rather than bilayer curvature alone [41]. Nevertheless, the curvature present in biological membranes is most likely essential to intracellular as well as intercellular communication (e.g., budding, fusion), which are

Author's personal copy

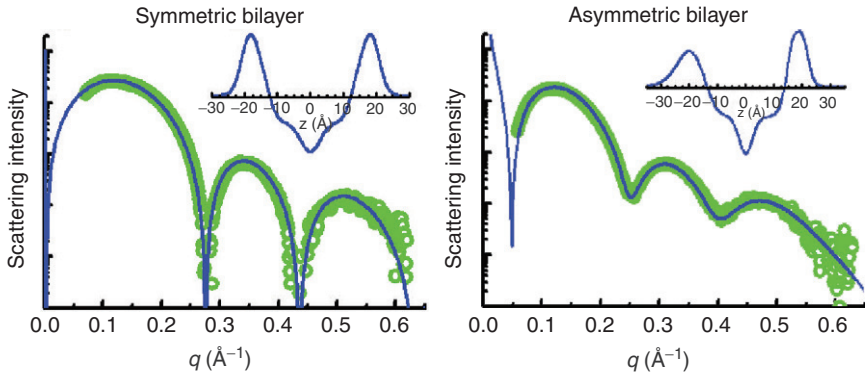

Figure 5 SAXS data from two different ULV systems. The scattering curves are clearly different in that the scattering function from symmetric zwitterionic bilayers (left hand panel) has zero minima, while the one from asymmetric charged bilayers (right hand panel) has nonzero minima. The insets to the figures contain the 1D electron density profiles (adapted from Ref. [41]).

accomplished only when certain geometrical conditions are present. Changes in the local curvature are also observed during the formation of lateral heterogeneities in model membranes and are expected to form lateral domains in biological membranes. The lateral organization and local curvature of membranes are also influenced by membrane proteins. On the other hand, curvature alone may enable mechanisms for organizing mobile molecules within the membrane [44].

Although it is not completely clear how the cell manages a membrane's lateral organization, the segregation induced by cholesterol is supposed to be a key factor in this process. For example, the sorting and trafficking of membrane proteins along the exocytic pathway through the Golgi apparatus has been linked to cholesterol and membrane thickness. Transmembrane domains of plasma membrane proteins have been found, on average, to be five amino acids longer than those of the Golgi, while membranes along the exocytic pathway increasingly thicken from the endoplasmic reticulum to the plasma membrane [45]. This progressive membrane thickening has been correlated with a concomitant increase in cholesterol content along the secretory pathway, suggesting that cholesterol determines the membrane's thickness and controls the destination of proteins by hydrophobic matching [28].

Thickening of lipid bilayers upon the addition of cholesterol has been observed in various lipid systems [46–48]. However, and perhaps more interesting, was the observation that cholesterol is not necessarily distributed symmetrically across bilayers, especially disordered bilayers [49].

Author's personal copy

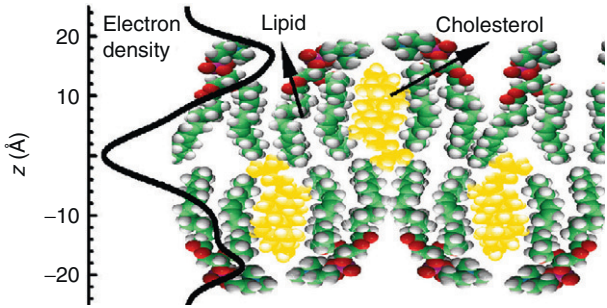

Figure 6 The asymmetric distribution of cholesterol between a bilayer's two leaflets containing short monounsaturated acyl chains (diC14:1PC) formed in 600 Å ULVs. The electron density profile on the left was obtained using SAXS data (adapted from Ref. [49]).

SAXS carried out on systems of monounsaturated lipid bilayers revealed that the cholesterol density ratio between a bilayer's two leaflets can be as high as two (Fig. 6). This asymmetry is especially true for bilayers made up of shorter acyl chain lipids with inherent increased disorder, and diminishes with increasing acyl chain length. As the same asymmetry was not observed for planar oriented bilayers [50], this result was attributed to the significant curvature present in the bilayers of 600 Å ULVs. This result is likely of relevance to biological membranes which consist of a wide variety of lipids with different intrinsic curvature properties. Although it is still not clear whether local curvature affects lipid composition, or vice versa, the resultant structural changes that may take place as a result of differing lipid properties may be important in how a membrane regulates protein function.

3.3. Advanced Bilayer Models Used in X-ray Scattering

Compared to neutron scattering, X-ray scattering offers the possibility of an extended range of measurable scattering intensity, thus permitting for the use of more complex models the bilayer ED profile contains features which cannot be described by simple step functions. Models with a constant ED would include physically unrealistic discontinuities that would lead to spurious large amplitude high q oscillations in the scattering form factor [51,52]. Although the simplest solution is to add more steps to the model, doing so unrealistically proliferates the number of parameters which may not even be accurate descriptors of the bilayer's molecular organization.

A better approach is to model the ED profile by some smooth function. For example, for a given q range Pabst *et al.* [53] utilized three Gaussians

Author's personal copy

each representing the polar headgroup (one in each leaflet) and the methyl terminus. Eq (10) can thus be rewritten as

$$\Delta\rho(z) = (\rho_{\mathrm{H}} - \rho_{\mathrm{W}})\left(\exp\left(-\frac{(z - z_{\mathrm{H}})^2}{2\sigma_{\mathrm{H}}^2}\right) + \exp\left(-\frac{(z + z_{\mathrm{H}})^2}{2\sigma_{\mathrm{H}}^2}\right)\right) + (\rho_{\mathrm{C}} - \rho_{\mathrm{W}})\exp\left(-\frac{z^2}{2\sigma_{\mathrm{C}}^2}\right), \tag{13}$$

where ρ_{W}, ρ_{H}, and ρ_{C} are the EDs of water, the headgroup, and the hydrocarbon tails, respectively, and z_{H}, σ_{H}, and σ_{C} are the position and widths of their corresponding Gaussians; note that $z_{\mathrm{C}} = 0$. The scattering intensity that corresponds to such a bilayer can then be expressed as

$$I_{\mathrm{B}}(q) = 2\pi\left[2\sigma_{\mathrm{H}}(\rho_{\mathrm{H}} - \rho_{\mathrm{W}})\exp\left(-\frac{(q\sigma_H)^2}{2}\right)\cos(qz_{\mathrm{H}}) + \sigma_{\mathrm{H}}(\rho_{\mathrm{C}} - \rho_{\mathrm{W}})\exp\left(-\frac{(q\sigma_{\mathrm{C}})^2}{2}\right)\right]^2. \tag{14}$$

This is most likely the simplest model of a lipid bilayer ED profile that captures its overall form. On the other hand, it also neglects features that might also may be important to some studies.

Wiener *et al.* [52] demonstrated that the essential feature of an ED model is its ability to accommodate an asymmetric headgroup by describing it with two Gaussians. In doing so, values of some data previously obtained from low-angle X-ray scattering studies (e.g., distance between the headgroups, D_{HH}) were improved. In other cases, however, either poor experimental resolution and/or the inherent disorder present in liquid crystalline bilayers precluded resolving a bilayer's detailed features. What was found to be important to most of the cases, however, was the plateau region between the headgroups and terminal methyls. This corresponds to the region of methylene-like groups (i.e., CH_2 and CH) whose ED is, in general, different from that of water. The inclusion of all of the above mentioned features in to one description resulted in the advanced hybrid models of a lipid bilayer.

A variety of structural models have been applied to describe the X-ray scattering data from lipid bilayers. The step function models are an over-simplified description of the bilayer's ED profiles, while the much more complicated structural models consist of too many parameters and are restricted to systems that are not fully hydrated [54]. A more successful model was developed by Nagle and coworkers [52]. This hybrid model

Author's personal copy

addressed the issues of the previous two, consisting both of Gaussian and step functions. However, the baseline created by the step functions proved to be an awkward aspect of this model, because the ED in the superposition region is not only the result of water molecules and hydrocarbon groups, but also contains parts of the phosphatidylcholine headgroup. A better model would represent the various groups by separate functions. Klauda *et al.* [55] demonstrated such a model through the use of three Gaussians (two for the headgroups and one for the terminal methyls) and two error functions (discussed in Section 3.1) for the water and the hydrocarbon chain regions. The mathematical description for such a model is then a combination of Eqs. (10) and (13), and (11) and (14).

With the development of more advanced models that utilize an increased number of free parameters, there is a need for more experimental data. Low-angle diffuse X-ray scattering from unoriented MLVs provided data up to 0.5 Å^{-1} [53], while fully hydrated aligned multilamellar samples resulted in continuous form factors up to 0.8 Å^{-1} [56,57]. However, in contrast to the usual crystallographic measurement of peak intensities or diffuse scattering from MLVs, the method by Lyatskaya *et al.* [56], and Liu and Nagle [57] did not adequately address the low q data. Later on Kučerka *et al.* [42] introduced a global analysis that combined data from ULVs and aligned samples, thus making good use of the data over the entire q range of scattering (Fig. 7).

3.4. Joint Refinement of Neutron and X-ray Scattering

The ED and NSLD models described above emphasize different but complementary features of the bilayer (compare Fig. 8A and B). It thus follows, that a combined approach should describe the structural features accentuated by each technique, but in a manner that addresses them simultaneously. This is illustrated in the way lipid area, A, is determined. For both X-ray and neutron scattering, A, is calculated using the bilayer's thickness and volumetric information. However, it should be stressed that the two techniques are sensitive to different bilayer thicknesses. The thickness best resolved by X-rays is the distance between the lipid headgroup phosphates, D_{HH}, while in the case of neutron scattering the high contrast between the protonated lipid and deuterated water accurately defines the total bilayer thickness, D_B. Even though they are the two most robust experimentally determined parameters, D_{HH} and D_B are not directly comparable, and neither on its own provides all of the desired bilayers structural information. Instead, models are used to determine the remaining structural parameters where better parameter determination should ensue when more data are included. The simultaneous analysis of X-ray and neutron scattering data results in parameters that better describe all the key bilayer features.

Author's personal copy

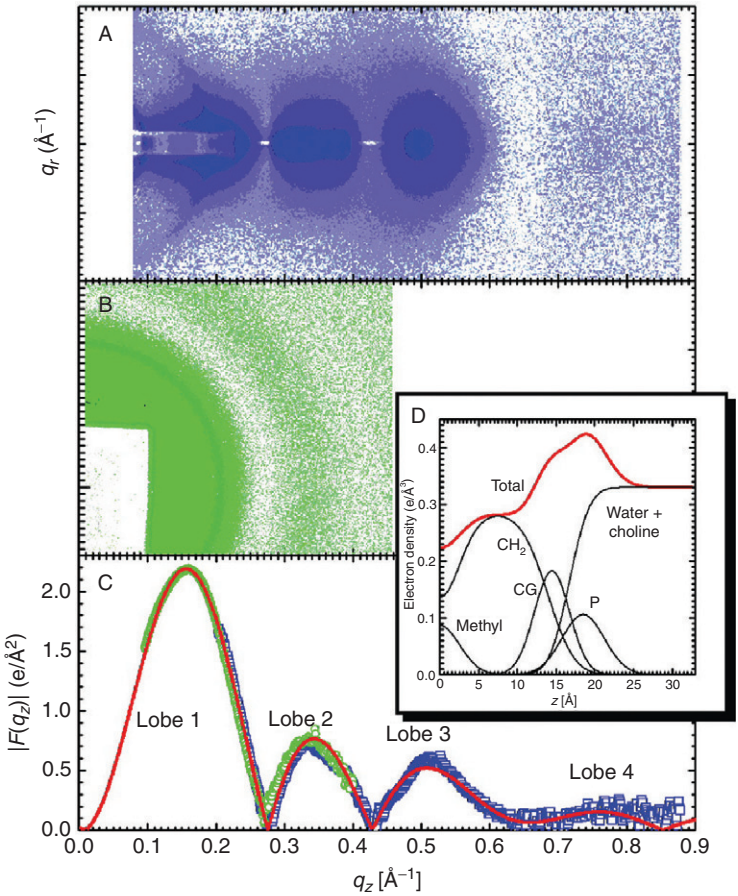

Figure 7 X-ray diffuse scattering from aligned multibilayers (A) and isotropic ULVs (B) in the fluid phase. (C) Global analysis combining the diffuse scattering data from aligned multibilayers (squares) and ULVs (circles). The solid line is the fit to the data using the hybrid model of electron density (ED) distribution across the bilayer. Inset to the figure (D) shows the one-dimensional ED of this model (solid line) and its decomposition into its various submolecular components (ED for half of the bilayer).

The joint refinement of X-ray and neutron diffraction data to obtain bilayer structural information was first reported by Wiener and White [54]. However, even though they used highly ordered, partially dehydrated multibilayers, those experiments illustrated the challenges faced by the diffraction method. Recently, Kučerka *et al.* [33] introduced a similar approach for calculating SDPs, where the simultaneously analyzed X-ray and neutron small-angle scattering data allow for the use of fewer parameters (by nearly 50%) to fit the data when compared to the

Author's personal copy

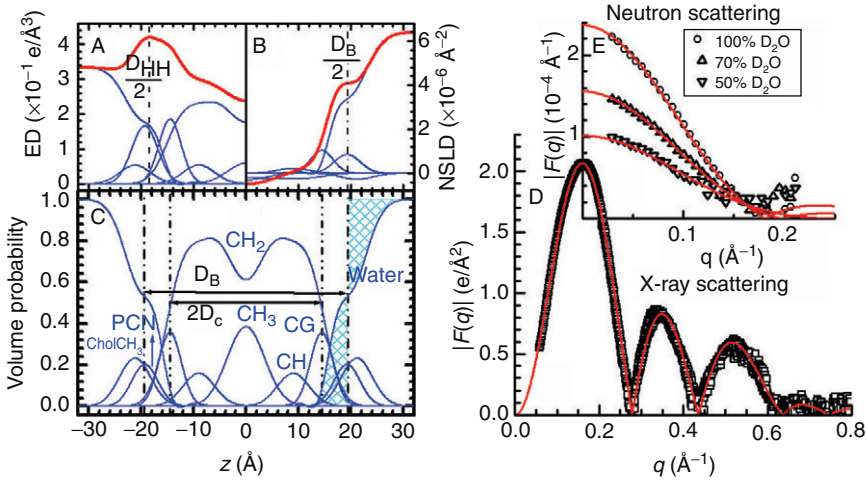

Figure 8 Illustration of lipid bilayer structure determination through the joint refinement of X-ray and neutron scattering data. The scattering density profile (SDP) model representation of a bilayer in real space is shown on the left, where the top panels show electron densities (ED) (A) and neutron scattering length densities (NSLD) (B) of the various lipid component distributions, including the total scattering density (thick lines). Panel (C) shows volume probability distributions, where the total probability is equal to 1 at each point across the bilayer. The point where the shaded areas are equal defines the Gibb's dividing surface between the lipid bilayer and the water phase (effectively D_B). Graphs on the right show the experimentally determined X-ray (D) and contrast varied neutron (E) scattering form factors (points) together with the best fits to the data (solid lines), as was shown in Ref. [60].

original composition-space model [58]. This analysis utilizes the continuous X-ray diffuse scattering from aligned multibilayers, observed at mid-to-high scattering vectors q (i.e., $0.2\ \text{Å}^{-1} < q < 0.8\ \text{Å}^{-1}$), and the diffuse scattering from isotropic ULVs, effectively extending the q range down to $\sim 0.05\ \text{Å}^{-1}$ (see Fig. 7), together with the contrast varied neutron scattering data from ULVs (Fig. 8D and E, respectively).

The biggest challenge in designing a good model is to ensure that it ultimately describes the main structural features of a bilayer. Although a model that represents each individual atom is certainly accurate, it would require the use of too many parameters for the available data. As such, in order to reduce the number of parameters, bringing it in line with the available data, the grouping of atoms into component groups is necessary. In the case of X-rays, the features with the most contrast are the electron-dense headgroups and the ED-low terminal methyl groups found in the bilayer center (Fig. 8A). In the case of neutrons, the greatest contrast is between the fully protonated lipids and the deuterated water (Fig. 8B). It is imperative that all of these features be included in a model that aims to simultaneously

Author's personal copy

describe both NSLD and ED profiles. The most parsimonious, but still adequate SDP model [33], has been shown to be comprised of the combined carbonyl and glycerol groups, which are described by a single Gaussian (CG), the phosphate group and part of the choline (CH_2CH_2N) by another Gaussian (PCN), and the remaining choline ($3\times CH_3$) by yet a third Gaussian ($CholCH_3$). The error function represents the total hydrocarbon region (i.e., sum of CH_2, CH, and CH_3 groups), where the CH and CH_3 groups are each described by a single Gaussian.

Although the SDP model is designed to obtain structure from X-ray and neutron scattering data, the primary description is not in terms of the ED or NSLD. Instead, it is described by volume probability distributions, $P_i(z)$ (Fig. 8C) which satisfy the spatial conservation principle, i.e., where volume is conserved. Compared to previous models based on global spatial conservation [59], the novel feature of the SDP model is that it imposes spatial conservation locally. This is accomplished through the water distribution (denoted by W) not being defined by any particular function, but is rather calculated on the basis of the "complementarity" requirement, whereby all of the probabilities add up to 1

$$P_{\mathrm{W}}(z) = 1 - P_{\mathrm{CG}}(z) - P_{\mathrm{PCN}}(z) - P_{\mathrm{CholCH_3}}(z) - P_{\mathrm{HC}}(z). \tag{15}$$

In this way, the model satisfies the spatial conservation principle, while capturing all of the features presented by the different SDPs [33] that are calculated as

$$\Delta\rho(z) = \sum(\rho_i - \rho_{\mathrm{W}})P_i(z), \tag{16}$$

where ρ_i represent the EDs or NSLDs of various components (i.e., CG, PCN, $CholCH_3$, CH, CH_2, CH_3).

In this case, where data from different sample preparations (i.e., aligned multilayers and ULVs) and probes (i.e., X-rays and neutrons) are combined, the scattering is more appropriately described by form factors as opposed to intensities. The form factors for the symmetric SDP model are then obtained from the Fourier transform

$$F(q) = 2\int_0^{D/2} \Delta\rho(z)\cos(qz)\,\mathrm{d}z, \tag{17}$$

where the integration extends from the bilayer center ($z = 0$) to a point $D/2$ beyond which $\Delta\rho(z) = 0$. The solid lines in Fig. 8D and E show X-ray and neutron scattering form factors, respectively, obtained through the use of the SDP model [60].

Author's personal copy

3.5. Lipid Area

The main purpose of models is to obtain structural information, among which the area per lipid, A, is one of the most important parameters that is needed to accurately describe bilayer structure, and lipid–lipid and lipid–protein interactions in biomembranes. However, A is not easily determined and is only obtainable if additional information is provided to constrain the many parameters that are required in any realistic model of a bilayer. It should be emphasized, however, that this is not a criticism for the use of models. On the contrary, the unique advantage of models is that information from other experiments can be used to refine them [55]. For example, total lipid volume, V_L, one of the most accurately known parameters can be included to reduce the total number of variables [61–63]. Even though the experimentally obtained scattering contains information about the bilayer's structure in the z direction (i.e., along the bilayer normal), the addition of V_L allows for the evaluation of structure in the lateral direction, namely A.

In the case of X-rays one of the most pronounced features in an ED profile are the electron-dense headgroups, providing the head–head spacing D_{HH} (see Fig. 8A) and from which the hydrocarbon chain region thickness, D_C, can be estimated using certain assumptions [32]. One assumption is that the distance between the headgroup phosphate and the hydrocarbon region (i.e., $D_{H1} = D_{HH} - D_C$) does not change for different lipids or as a function of temperature. It then follows that

$$A = (V_L - V_{HL})/(D_{HH} - D_{H1}), \tag{18}$$

where V_{HL} is the volume of lipid headgroup.

In the case of neutrons, the greatest contrast is between the fully protonated lipids and the deuterated water, resulting in the water distribution function—effectively the Gibbs dividing surface for the water region. The position of the Gibbs dividing surface is defined by the equality of the integrated water probabilities to its left and the integrated deficit of water probabilities to its right (Fig. 8C, shaded areas). In other words, it is the position that would correspond to the edge of the distribution if it was represented by a simple box model, making it equivalent to Luzzati's division of two component systems consisting of water and lipid [60]. This criterion then directly yields [33] a simple equation for calculating lipid area

$$A = 2V_L/D_B. \tag{19}$$

It should be emphasized that Eq. (19) implies that neutron scattering is a more appropriate technique for determining parameters such as A, while

Author's personal copy

Table 2 Lipid bilayer structural data obtained from the joint refinement of X-ray and neutron scattering data [33,60,64]

Lipid	T (°C)	D_{HH} (Å)	$2D_C$ (Å)	D_B (Å)	A (Å^2)
diC16:0PC	50	38.0	28.4	39.0	63.1
di4MeC16:0PC	30	36.4	27.2	35.4	80.5
diC14:1PC	30	29.6	23.4	33.7	64.2
diC16:1PC	30	32.1	26.2	36.2	65.8
diC18:1PC	30	36.8	29.0	38.9	66.9
diC20:1PC	30	38.9	32.6	42.5	66.6
diC22:1PC	30	45.5	36.4	46.4	65.7
diC24:1PC	30	47.9	41.6	52.2	62.7

high resolution X-ray scattering reveals more detailed intrabilayer structural information. By simultaneously analyzing the two different data sets one can then better determine the precise structure of fully hydrated, liquid crystalline bilayers. Importantly, the new analysis indicated that areas (see Table 2) for some lipids have been overestimated by as much as 10% when only X-ray scattering was used to determine A.

The inconsistencies in lipid areas found in the literature have also been highlighted by the disparate results arising from MD simulations that use different force fields. For example, MD simulations based on CHARMM (Chemistry at HARvard molecular mechanics) potentials are performed at nonzero surface tension in order that they may better agree with X-ray scattering data [55], whereas simulations using a combination of GROMOS and OPLS (Optimized potential for liquid simulations) potentials do not seem to require this additional "tweaking" [65]. It is noteworthy to emphasize that in addition to comparing modeling results, MD simulations should be directly compared to scattering data [55,66–69]. As MD force fields are considered to be "well tuned" only if they are able to reproduce experimental data, thus much more work is needed to reconcile simulation and experiment, even in the simplest case of single-component membranes.

4. Scattering from Laterally Heterogeneous ULVs

Because of their biological implications, the discovery of functional domains or "rafts" in cell membranes has stimulated considerable interest with regard to the lateral organization of both cell and model membranes. Our current understanding of rafts comes from studies of lateral phase separation in model bilayers composed of ternary mixtures of saturated and unsaturated lipids, including cholesterol. Formation of these domains

Author's personal copy

is assumed to be the result of distinct interactions between cholesterol and lipids, with different hydrocarbon chains causing cholesterol to partition preferentially with saturated hydrocarbon chain lipids, forming a liquid ordered phase [70]. The high affinity of cholesterol for saturated lipids, or more precisely, the large difference in cholesterol affinities for different lipid species is considered to be the driving force for the formation of cholesterol rich domains [71]. However, looking at it from a different point of view, one can argue that rather than cholesterol's differing affinities for different types of lipids, domain formation may be the result of the aversion between the two lipid species for each other, supporting the notion of lipid-driven domain formation [72].

A variety of approaches have been used to characterize lateral heterogeneities. Of the different techniques the visually based approaches outnumber the scattering techniques, most likely because some may find the analysis used to interpret scattering data, onerous. However, once the methods of analyses have been dealt with, X-ray and neutron scattering offer the possibility of resolving features on the order of nanometers, while at the same time yielding ensemble-averaged information. Importantly, SANS utilizes selective lipid deuteration as a method of contrast enhancement, whereas the inclusion of bulky fluorescent dyes or labels used by many of the optical techniques (e.g., fluorescence microscopy), can alter the system's phase behavior [73].

The detection of domains using SANS depends on the use of contrast variation. First, the contrast between the overall vesicle and the solution is minimized through the appropriate use of H_2O and D_2O. This minimum contrast condition takes place when the NSLD of the hydration medium is equal to that of the vesicle [74]. Second, the contrast between domains of different composition is enhanced by the selective deuteration of a lipid that preferentially partitions into one phase over the other. Figure 9 shows a rise in scattering intensity when lateral segregation takes place. The domains or heterogeneities in the ULVs have NSLDs that are different from the mean NSLD resulting in contrast between the domains and the water (H_2O/D_2O) [75].

4.1. Model-Independent Analysis

As in the case of homogeneous ULVs it is possible to evaluate domains or lateral heterogeneities from SANS data without having to rely on precise models (see Section 2). The mean square fluctuation in the NSLD is the Porod invariant, Q, and can be related to the integral of the scattering intensity ($Q = \int I(q) q^2 \, dq$) [8,9]. However, Q in this case depends on both the radial and lateral fluctuations (i.e., inhomogeneities) in the NSLD. The membrane's total NSLD can be expressed as a sum of three contributions

Author's personal copy

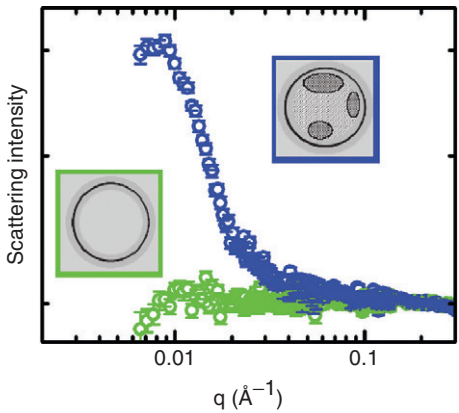

Figure 9 Schematic representation of the sensitivity of SANS to lateral inhomogeneities. The curve at the bottom corresponds to the scattering from a contrast matched homogeneous bilayer ULV (inset, bottom left corner), while the top curve exhibits an additional contribution to the scattered intensity arising from the contrast between the lateral domains and the remaining ULV (inset, top right corner).

$$\Delta\rho(r,\theta,\varphi) = \Delta\rho_{\text{mean}} + \rho_{\text{rad}}(r) + \rho_{\text{lat}}(r,\theta,\varphi), \tag{20}$$

where $\Delta\rho_{\text{mean}}$ is the mean NSLD contrast, $\rho_{\text{rad}}(r)$ is a component that fluctuates radially (discussed in Section 3) but does not vary with θ and φ, and $\rho_{\text{lat}}(r,\theta,\varphi)$ is the fluctuating component of NSLD that describes the membrane's lateral heterogeneities on the ULV's surface [76]. The scattering intensity can then be decomposed using the same terms as above. The Porod invariant can thus be written as

$$Q = Q_{\text{mean}} + Q_{\text{rad}} + Q_{\text{lat}}. \tag{21}$$

Q_{mean} corresponds to the square of the mean NSLD contrast, Q_{rad} corresponds to the mean square radial fluctuations, and Q_{lat} corresponds to the mean square lateral fluctuations in the NSLD [76].

Although this approach applies to small-angle scattering in general, it lends itself ideally to SANS, particularly because of the unique sensitivity of neutrons to H/D substitution and the possibility to nullify or enhance scattering contrast. For example, the leading term in Eq. (21) can be eliminated through the appropriate mixture of H_2O/D_2O. Under contrast matched conditions (i.e., $\Delta\rho_{\text{mean}} = 0$) the total scattering consists solely of contributions from the radial and lateral fluctuations in the NSLD, while Q_{mean} diminishes (see Fig. 10).

Figure 10 shows plots of the Porod invariant calculated for ULVs with different lipid deuteration ratios. While the minimization of the Q_{mean}

Author's personal copy

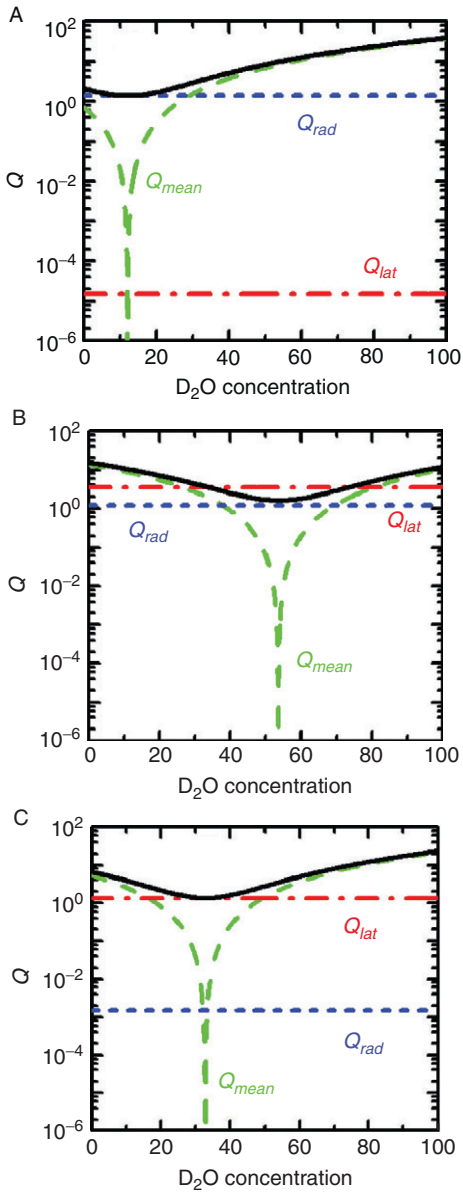

Figure 10 The Porod invariant, Q, and its components plotted for a 1:1 mixture of DPPC:DLPC as a function of D_2O concentration. The graphs correspond to the three ratios of deuterated-to-nondeuterated DPPC lipid: (A) 0:100, (B) 100:0, and (C) 50:50 (adapted from Ref. [76]).

Author's personal copy

contribution is achieved by the straightforward manipulation of H_2O/D_2O, the separation of Q_{rad} and Q_{lat} is not as simple and requires some knowledge of the structure and chemical composition of the membrane. As Q_{rad} arises from the contrast between the mean lipid acyl chain NSLD and the mean lipid headgroup NSLD, and Q_{lat} depends on the contrast between the lipid's acyl chains, it is then obvious that the relative contributions of the two depend on the deuteration ratio of the lipid chains. The extent of NSLD contrast between the two domains (one rich in DLPC, 1,2-dilauroyl-*sn*-glycero-3-phosphocholine, and other one rich in DPPC, 1,2-dipalmitoyl-*sn*-glycero-3-phosphocholine) that corresponds to Q_{lat} has a minimum when all DPPC hydrocarbon chains are protonated (Fig. 10A) and reaches a maximum value when they are all deuterated (Fig. 10B). On the other hand, the large NSLD contrast between lipid headgroups and acyl chains prevents the unambiguous subtraction of Q_{rad} for both of these cases. However, the latter contribution reaches a minimum when the ratio of deuterated-to-nondeuterated DPPC is 50% (Fig. 10C). This then allows for the reasonably facile determination of the Q_{lat} contribution. Figure 10C shows that the value of Q_{lat} near the contrast match point is essentially equal to the total Q [76].

The formation of domains and the concomitant identification of phase boundaries as a function of either membrane composition or temperature can be detected in changes to Q. However, Q alone cannot be used to determine more precise details of heterogeneous vesicles. Consequently, the determination of parameters such as, domain area fraction and composition still relies on fitting experimental data with the appropriate analytic form factor.

4.2. Full Form Factor

The general findings from fluorescent microscopy studies suggest that the formation of domains depends on both membrane composition and temperature, and that their shapes exhibit various morphologies depending on the thermodynamic phases of the components [77]. Nevertheless, in the liquid–liquid coexistence phase, the most likely equilibrium state consists of ULVs with single circular domains [78]. Note however, that the assumption of completely segregated circular domains is not a necessary condition. As ULVs undergo rotational diffusion over the course of an experiment, SANS results are thus a description of an orientational and ensemble average. This means that the results obtained using the single circular domain approximation provide information regarding the circular-domain-equivalent of membrane heterogeneities.

As shown in Fig. 11 the NSLD of a heterogeneous ULV is axially symmetric [i.e., $\rho(r,\theta,\varphi) = \rho(r,\theta)$] and can be represented in spherical coordinates (i.e., r and θ) by a function that is equal to $\rho_{ld}(r)$ in the liquid

Author's personal copy

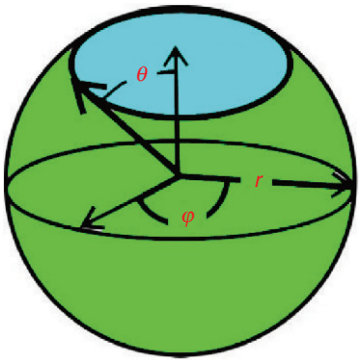

Figure 11 Schematic of a heterogeneous vesicle, where the circular domain is centered on the vesicle's z axis (adapted from Ref. [79]).

disordered (ld) phase region and $\rho_{lo}(r)$ in the liquid ordered (lo) phase region, where the domain is bounded by an angle α. This definition makes $\Delta\rho_{mean} + \rho_{rad}(r)$ from Eq. (20) equal to $\rho_{ld}(r) - \rho_W$ over the entire surface of the vesicle, and $\rho_{lat}(r,\theta)$ equals to $\rho_{lo}(r) - \rho_{ld}(r)$ in the domain region (i.e., $\theta \leq \alpha$), while $\rho_{lat}(r,\theta)$ is zero everywhere else.

Although the calculation of the scattered intensity from a heterogeneous ULV is more complicated (compared to Eq. (8)), it can still be resolved analytically by expanding the scattering potential into spherical harmonics using a convenient frame of reference (see Ref. [79] for more details). This derivation assumes sharp boundaries between the two phases and that the NSLD is separated into radial and angular components (i.e., $\rho(r,\theta) = \rho_{rad}(r)\rho_{ang}(\theta)$). Then, as in the previous case of model-independent analysis (Section 4.1), the scattering intensity can be decomposed in to three different components that reflect the three components of the NSLD function (see Eq. (20)). The total scattered intensity from a heterogeneous ULV of radius R can then be written as [79]

$$I(q,R) = \left(2Z_{mean}(q,R) + 2Z_{rad}(q,R) + Z_{lat,0}(q,R)X_0(\alpha)\right)^2 + \sum_l (2l+1)^2 Z_{lat,l}^2(q,R)X_l^2(\alpha). \tag{22}$$

Here, $Z_{mean}(q,R)$ corresponds to the scattering arising from the contrast between the mean NSLD of the vesicle, ρ_{mean}, and that of medium, ρ_W,

$$Z_{mean}(q,R) = \int_{R-d/2}^{R+d/2} 4\pi r^2(\rho_{mean} - \rho_w)\frac{\sin(qr)}{qr}\,dr, \tag{23}$$

Author's personal copy

and $Z_{\mathrm{rad}}(q,R)$ corresponds to the scattering due to the radial variations in the NSLD

$$Z_{\mathrm{rad}}(q,R) = \int_{R-d/2}^{R+d/2} 4\pi r^2 \rho_{\mathrm{rad}}(r) \frac{\sin(qr)}{qr} \mathrm{d}r. \tag{24}$$

Both of these contributions together determine the scattering form factor from a homogeneous vesicle. This is equivalent to Eq. (8).

The scattering due to the lateral contrast between the two phases is incorporated through the functions $Z_{\mathrm{lat},\,l}(q,R)$ and $X_l(\alpha)$ that are calculated within the boundaries of the domain (where $\rho_{\mathrm{lat}}(r,\theta) = \rho_{\mathrm{lo}}(r) - \rho_{\mathrm{ld}}(r)$) as [79]

$$Z_{\mathrm{lat},l}(q,R) = \int_{R-d/2}^{R+d/2} 4\pi r^2 \rho_{\mathrm{lat}}(r,\theta) j_l(qr)\, \mathrm{d}r, \tag{25}$$

and

$$X_0(\alpha) = 1 - \cos(\alpha) \tag{26}$$

and

$$X_l(\alpha) = \frac{\cos(\alpha) P_l(\cos(\alpha)) - P_{l+1}(\cos(\alpha))}{l}, \quad l = 0, \tag{27}$$

where j_l and P_l are spherical Bessel functions and Legendre polynomials of order l, respectively. Note that for the typical case of polydisperse ULVs, it is important to integrate Eq. (22) over the vesicle size distribution as suggested by Eq. (7). This can be done following the approach of SFF and Laplace transforms described in Ref. [79].

The lipid membrane, even in the case of a laterally homogeneous vesicle, typically has an NSLD profile that varies across the bilayer (see Section 3). In the simplest representation there are, at a minimum, differences between the lipid headgroup and acyl chain regions, as was discussed in Section 3.1. On the other hand, the discussion in Section 4.1 outlines the experimental possibility of producing ULVs with a radially homogeneous NSLD profile through the partial deuteration of the lipid acyl chains. According to Fig. 10, such a contrast condition provides the best possibility for separating radial and lateral scattering components. In addition, it is also possible to nullify the contribution of the Z_{mean} form factor by utilizing the appropriate H_2O/D_2O mixture, such that $\rho_{\mathrm{mean}} = \rho_{\mathrm{W}}$. By doing so, this results in the optimal condition for detecting and characterizing domains.

Author's personal copy

4.3. The Influence of Curvature on Domains

As was discussed, the optimal conditions for the detection and characterization of membrane domains are significantly different from those that are optimal for the measurement of the vesicle form factor used for the purpose of determining vesicle size and/or membrane transverse structure (Section 3). While the vesicle form factor is obtained from scattering measurements of protonated ULVs in 100% D_2O, domains are best observed at the contrast matched condition (Section 4.1). It is nevertheless equally important to have access to both conditions, something that is conveniently achieved by SANS.

An interdependence between local curvature and membrane structure has been observed in model membranes in both the transverse (see Section 3.2) and recently, in the lateral directions [80]. Lateral direction measurements were performed using two contrast conditions allowing for a separate assessment of the vesicle form factor and any contributions to the scattering from lateral heterogeneities. Figure 12 emphasizes the

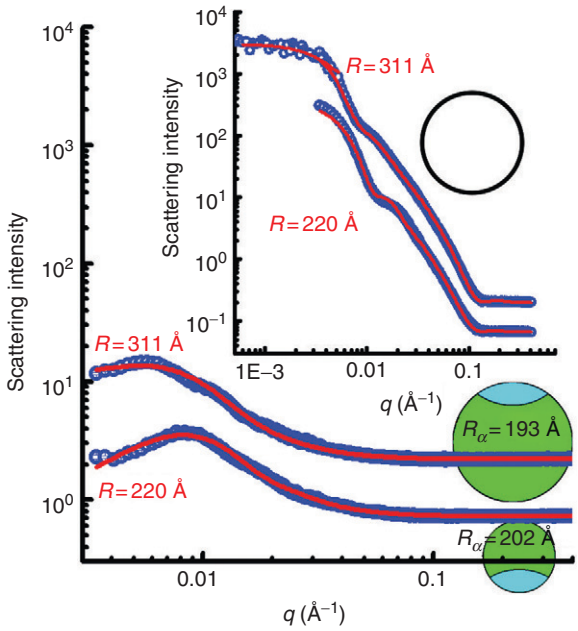

Figure 12 SANS curves obtained from heterogeneous vesicles. The top part shows measurements performed at the contrast condition that enhances the vesicular form factor (i.e., Z_{mean} and Z_{rad}), while the contrast condition at the bottom accentuates the contribution from lateral heterogeneities (i.e., Z_{lat} and X).

Author's personal copy

significant differences between SANS intensities for these two cases. Overall, vesicle features (e.g., size and shape) are obtained when the Z_{mean} contribution (see Eq. (22)) is accentuated by the large contrast made possible between the fully deuterated water and the fully protonated lipid vesicles. Under these contrast conditions, lipid lateral heterogeneity does not produce significant lateral variations in the NSLD and consequently, the data can be successfully analyzed using the homogeneous vesicle form factor.

The bottom of Fig. 12 shows SANS data obtained at the contrast condition where lateral heterogeneities are accentuated. The radial variation of the NSLD, reflected in Z_{rad}, was minimized by utilizing a mixture of protonated and deuterated lipids such that the lipid acyl chain NSLD was equal to that of the headgroups. In addition, ULVs were dispersed in 36% D_2O solution to minimize the contribution of Z_{mean}. As the remaining terms in Eq. (22) depend predominantly on the difference between the NSLDs of the two phases, it is possible to detect and characterize the formation of domains. Equation (22) defines the domain size by the angle α. The spherical cap area is calculated as

$$a = 2\pi R^2(1 - \cos(\alpha)), \tag{28}$$

and the apparent domain radius is defined via the planar projection as

$$R_\alpha = \sqrt{\frac{2(1 - \cos(\alpha))}{\pi}}R, \tag{29}$$

where R is the radius of the vesicle. Pencer *et al.* [80] discovered that the apparent size of the circular domain decreased slightly with increasing vesicle radius, and revealed more a substantial change when compared to the vesicle size. This result may imply that the demixing of lipids depends on vesicle size and thus on membrane curvature.

There is ongoing controversy regarding the size and stability of membrane domains in both cell and model membranes. This controversy is further complicated by the variability in sensitivity among the different techniques used to detect domains, and by the different model membrane systems used. In particular, the observation of lateral heterogeneities in ULVs by fluorescence resonance energy transfer (FRET), where none was observed in GUVs by fluorescence microscopy (FM), has led to fundamental questions regarding the nature and existence of membrane domains [81]. However, the possibility for studying lateral membrane heterogeneities using a single experimental technique has helped to reconcile these apparent discrepancies. The recently developed SANS approach has clearly shown that membrane curvature has an important role to play in

Author's personal copy

the miscibility of the various lipid components [80]. It therefore seems that the apparent inconsistencies between ULV FRET and GUV FM studies may merely be due to differences in membrane curvature.

5. Concluding Remarks

Over the years many of the most important properties of lipids have been determined through various physical techniques. In the mean time, the plasma membrane has been shown to be considerably more complex than originally thought, especially with regard to the diversity of lipids and their unique functions. Although the importance of proteins in biology has been known for some time now, the importance of lipids in general and their role in protein function in particular—through functionalised lipid platforms - has been a recent phenomenon. Even though scattering techniques in the past have played a role in evaluating lipid–lipid and lipid–protein relationships, recent advances in the analysis of small-angle scattering data have opened doors for understanding these relationships that were not previously imaginable, even a decade ago.

In this chapter, we presented some of the basic scattering principles together with some of the latest developments regarding the application of small-angle X-ray and neutron scattering methods used to explore the structure of biologically relevant membranes. The possibilities of model-independent approaches have been demonstrated in the case of model membranes with homogeneous as well as heterogeneous lateral structures. In particular, the latter case lends itself ideally to neutron scattering methods because of the unique sensitivity of neutrons to H/D substitution and the possibility to nullify or enhance scattering contrast. On the other hand, high resolution X-ray scattering data have been shown to be well suited for the detailed internal structure of lipid bilayers using model dependent analysis to elucidate the bilayer's transverse structure. Structural biophysics is evolving to take advantage of recent developments in small-angle scattering to accurately determine the structure of lipid bilayers that will help to reveal the numerous relationships between structure and function in biological membranes.

REFERENCES

[1] S.J. Singer, G.L. Nicolson, The fluid mosaic model of the structure of cell membranes, Science 175 (1972) 720–731.

[2] A.M. Dopico, G.J. Tigyi, *Methods in Membrane Lipids—Methods in Molecular Biology, Vol. 400* Humana Press, Totowa, NJ, 2007.

Author's personal copy

[3] T.A. Harroun, N. Kučerka, M.-P. Nieh, J. Katsaras, Neutron and X-ray scattering for biophysics and biotechnology: examples of self-assembled lipid systems, Soft Matter 5 (2009) 2694–2703.
[4] J. Fitter, T. Gutberlet, J. Katsaras, Neutron Scattering in Biology: Techniques and Applications, Springer, Berlin, 2006.
[5] J. Katsaras, J. Pencer, M.-P. Nieh, T. Abraham, N. Kučerka, T.A. Haroun, Neutron and X-ray scattering from isotropic and aligned membranes, in: K. Nag (Ed.), Structure and Dynamics of Membranous Interfaces John Wiley & Sons, Inc., Hoboken, NJ, 2008, pp. 107–134.
[6] J. Als-Nielsen, D. McMorrow, Elements of Modern X-Ray Physics, John Wiley & Sons, Ltd, Chichester, 2001.
[7] A. Guinier, G. Fournet, C.B. Walker, K.L. Yudowitch, Small Angle Scattering of X-rays, John Wiley & Sons Inc., New York, 1955.
[8] O. Glatter, O. Kratky, Small Angle X-ray Scattering, Academic Press, London, 1982.
[9] G. Porod, Die Röntgenkleinwinkelstreuung von dichtgepackten kolloiden Systemen - I, Teil. Kolloid Zeitschrift 124 (1951) 83–114.
[10] J.S. Huggins, H.C. Beniot, Form factors, Polymers and Neutron Scattering Oxford University Press Inc., New York, 1994, pp. 165–174.
[11] M.-P. Nieh, C. Glinka, S. Krueger, R.S. Prosser, J. Katsaras, SANS study on the effect of lanthanide ions and charged lipids on the morphology of phospholipid mixtures, Biophys. J. 82 (2002) 2487–2498.
[12] H. Frielinghaus, Small angle scattering model for multilamellar veiscles, Phys. Rev. E 76 , 2007; 051603.
[13] J.R. Nordlund, C.F. Schmidt, P.W. Holloway, T.E. Thompson, Effect of cytochrome b5 on the transbilayer distribution of phospholipids in model membranes, Biochemistry 21 (1982) 2820–2825.
[14] N. Düzgüneş, J. Wilschut, K. Hong, R. Fraley, C. Perry, D.S. Friend, T.L. James, D. Papahadjopoulos, Physicochemical characterization of large unilamellar phospholipid vesicles prepared by reverse-phase evaporation, Biochim. Biophys. Acta—Biomembr. 732 (1983) 289–299.
[15] M.-P. Nieh, V.A. Raghunathan, S.R. Kline, T.A. Harroun, C.-Y. Huang, J. Pencer, J. Katsaras, Spontaneously formed unilamellar vesicles with path-dependent size distribution, Langmuir 21 (2005) 6656–6661.
[16] W. Li, T.H. Haines, Uniform preparations of large unilamellar vesicles containing anionic lipids, Biochemistry 25 (1986) 7477–7483.
[17] B. Demé, M. Dubios, T. Gulik-Krzywicki, T. Zemb, Giant collective fluctuations of charged membranes at the lamellar-to-vesicle unbinding transition. 1. Characterization of a new lipid morphology by SANS, SAXS, and electron microscopy, Langmuir 18 (2002) 997–1004.
[18] E.W. Kaler, K.L. Herrington, A.K. Murthy, J.A.N. Zasadzinski, Phase behavior and structures of mixtures of anionic and cationic surfactants, J. Phys. Chem. 96 (1992) 6698–6707.
[19] S. Svenson, Controlling surfactant self-assembly, Curr. Opin. Colloid Interface Sci. 9 (2004) 201–212.
[20] M. Almgren, S. Rangelov, Spontaneously formed nonequilibrium vesicles of cetyltrimethylammonium bromide and sodium octyl sulfate in aqueous dispersions, Langmuir 20 (2004) 6611–6618.
[21] J. Leng, S.U. Egelhaaf, M.E. Cates, Kinetics of the micelle-to-vesicle transition: aqueous lecithin-bile salt mixtures, Biophys. J. 85 (2003) 1624–1646.
[22] M.-P. Nieh, T.A. Harroun, V.A. Raghunathan, C.J. Glinka, J. Katsaras, Concentration-independent spontaneously forming biomimetic vesicles, Phys. Rev. Lett. 91 , 2003; 158105.

Author's personal copy

[23] M.-P. Nieh, T.A. Harroun, V.A. Raghunathan, C.J. Glinka, J. Katsaras, Spontaneously formed monodisperse biomimetic unilamellar vesicles: the effect of charge, dilution, and time, Biophys. J. 86 (2004) 2615–2629.
[24] Y.I. González, H. Nakanishi, M. Stjerndahl, E.W. Kaler, Influence of pH on the micelle-to-vesicle transition in aqueous mixtures of sodium dodecyl benzenesulfonate with histidine, J. Phys. Chem. B 109 (2005) 11675–11682.
[25] P. Lesieur, M.A. Kiselev, L.I. Barsukov, D. Lombardo, Temperature-induced micelle to vesicle transition: kinetic effects in the DMPC/NaC system, J. Appl. Crystallogr. 33 (2000) 623–627.
[26] M.-P. Nieh, N. Kučerka, J. Katsaras, Spontaneously formed unilamellar vesicles, in: N. Düzgüneş (Ed.), Methods in Enzymology, Vol. 546 Academic Press Elsevier Inc., Burlington, 2009, pp. 3–20.
[27] A.G. Lee, How lipids affect the activities of integral membrane proteins, Biochim. Biophys. Acta 1666 (2004) 62–87.
[28] T.A. Harroun, W.T. Heller, T.M. Weiss, L. Yang, H.W. Huang, Experimental evidence for hydrophobic matching and membrane-mediated interactions in lipid bilayers containing gramicidin, Biophys. J. 76 (1999) 937–945.
[29] J. Karlovská, D. Uhríková, N. Kučerka, J. Teixeira, F. Devínsky, I. Lacko, P. Balgavý, Influence of N-dodecyl-N, Ndimethylamine N-oxide on the activity of sarcoplasmic reticulum Ca2+-transporting ATPase reconstituted into diacylphosphatidylcholine vesicles: effects of bilayer physical parameters, Biophys. Chem. 119 (2006) 69–77.
[30] J. Pencer, F.R. Hallett, Small-angle neutron scattering from large unilamellar vesicles: an improved method for membrane thickness determination, Phys. Rev. E 61 (2000) 3003–3008.
[31] G. Büldt, H.U. Gally, A. Seelig, J. Seelig, G. Zaccai, Neutron diffraction studies on selectively deuterated phospholipid bilayers, Nature 271 (1978) 182–184.
[32] T.J. McIntosh, S.A. Simon, Area per molecule and distribution of water in fully hydrated dilauroylphosphatidylethanolamine bilayers, Biochemistry 25 (1986) 4948–4952.
[33] N. Kučerka, J.F. Nagle, J.N. Sachs, S.E. Feller, J. Pencer, A. Jackson, J. Katsaras, Lipid bilayer structure determined by the simultaneous analysis of neutron and X-ray scattering data, Biophys. J. 95 (2008) 2356–2367.
[34] N. Kučerka, J.F. Nagle, S.E. Feller, P. Balgavý, Models to analyze small-angle neutron scattering from unilamellar lipid vesicles, Phys. Rev. E 69 , 2004; 051903(1–9).
[35] M. Schalke, P. Kruger, M. Weygand, M. a Lösche, Submolecular organization of DMPA in surface monolayers: beyond the two-layer model, Biochim. Biophys. Acta 1464 (2000) 113–126.
[36] S. Komura, Y. Toyoshima, T. a Takeda, Neutron small-angle scattering from single-walled liposomes of egg phosphatidylcholine, Jpn. J. Appl. Phys. 21 (1982) 1370–1372.
[37] M. Gradzielski, H. a Hoffmann, Structural investigations of charged o/w microemulsion droplets, Adv. Colloid Interface Sci. 42 (1992) 149–173.
[38] L.A. Feigin, D.I. a Svergun, Structure Analysis by Small-Angle X-ray and Neutron Scattering, Plenum Publishing Corporation, New York, 1987.
[39] M.A. Kiselev, P. Lesieur, A.M. Kisselev, D. Lombardo, V.L. Aksenov, Model of separated form factors for unilamellar vesicles, J. Appl. Phys. A 74(Suppl.) (2002) S1654–S1656.
[40] J. Pencer, S. Krueger, C. Adams, J. Katsaras, Method of separated form factors for polydisperse vesicles, J. Appl. Cryst. 39 (2006) 293–303.
[41] N. Kučerka, J. Pencer, J. Sachs, J. Nagle, J. Katsaras, Curvature effect on the structure of phospholipid bilayers, Langmuir 23 (2007) 1292–1299.
[42] N. Kučerka, Y. Liu, N. Chu, H.I. Petrache, S. Tristram-Nagle, J.F. a Nagle, Structure of fully hydrated fluid phase DMPC and DLPC lipid bilayers using X-ray scattering

Author's personal copy

from oriented multilamellar arrays and from unilamellar vesicles, Biophys. J. 88 (2005) 2626–2637.
[43] M.R. Brzustowicz, A.T. a Brunger, X-ray scattering from unilamellar lipid vesicles, J. Appl. Cryst. 38 (2005) 126–131.
[44] R. Parthasarathy, J.T. a Groves, Curvature and spatial organization in biological membranes, Soft Matter 3 (2007) 24–33.
[45] M.S. Bretscher, S. Munro, Cholesterol and the Golgi apparatus, Science 261 (1993) 1280–1281.
[46] D.L. Worcester, N.P. a Franks, Structural analysis of hydrated egg lecithin and cholesterol bilayers. II. Neutron diffraction, J. Mol. Biol. 100 (1976) 359–378.
[47] T.J. McIntosh, The effect of cholesterol on the structure of phosphatidylcholine bilayers, Biochim. Biophys. Acta 513 (1978) 43–58.
[48] J. Gallová, D. Uhríková, N. Kučerka, J. Teixeira, P. Balgavý, Hydrophobic thickness, lipid surface area and polar region hydration in monounsaturated diacylphosphatidylcholine bilayers. SANS study of effects of cholesterol and beta-sitosterol in unilamellar liposomes, Biochim. Biophys. Acta 1778 (2008) 2627–2632.
[49] N. Kučerka, M.-P. Nieh, J. a Katsaras, Asymmetric distribution of cholesterol in unilamellar vesicles of monounsaturated phospholipids, Langmuir 25 (2009) 13522–13527.
[50] N. Kučerka, J. Perlmutter, J. Pan, S. Tristram-Nagle, J. Katsaras, J.N. Sachs, The effect of cholesterol on short- and long-chain monounsaturated lipid bilayers as determined by molecular dynamics simualtions and x-ray scattering, Biophys. J. 95 (2008) 2792–2805.
[51] M.H.F. Wilkins, A.E. Blaurock, D.M. Engelman, Bilayer structure in membranes, Nat. New Biol. 230 (1971) 72–76.
[52] M.C. Wiener, R.M. Suter, J.F. Nagle, Structure of the fully hydrated gel phase of dipalmitoylphosphatidylcholine, Biophys. J. 55 (1989) 315–325.
[53] G. Pabst, M. Rappolt, H. Amenitsch, P. Laggner, Structural information from multilamellar liposomes at full hydration: full q-range fitting with high quality x-ray data, Phys. Rev. E 62 (2000) 4000–4009.
[54] M.C. Wiener, S.H. White, Fluid bilayer structure determination by the combined use of x-ray and neutron diffraction. I. Fluid bilayer models and the limits of resolution, Biophys. J. 59 (1991) 162–173.
[55] J.B. Klauda, N. Kučerka, B.R. Brooks, R.W. Pastor, J.F. Nagle, Simulation-based methods for interpreting X-ray data from lipid bilayers, Biophys. J. 90 (2006) 2796–2807.
[56] Y. Lyatskaya, Y. Liu, S. Tristram-Nagle, J. Katsaras, J.F. Nagle, Method for obtaining structure and interactions from oriented lipid bilayers, Phys. Rev. E 63, 2001; 011907(1–9).
[57] Y. Liu, J.F. Nagle, Diffuse scattering provides material parameters and electron density profiles of biomembranes, Phys. Rev. E. 69 , 2004; 040901 (1–4).
[58] M.C. Wiener, S.H. White, Fluid bilayer structure determination by the combined use of X-ray and neutron diffraction. II. "composition-space" refinement method, Biophys. J. 59 (1991) 174–185.
[59] J.F. Nagle, M.C. Wiener, Relations for lipid bilayers. Connection of electron density profiles to other structural quantities, Biophys. J. 55 (1989) 309–313.
[60] N. Kučerka, J. Gallová, D. Uhríková, P. Balgavý, M. Bulacu, S.J. Marrink, J. Katsaras, Areas of monounsaturated diacylphosphatidylcholines, Biophys. J. 97 (2009) 1926–1932.
[61] J.F. Nagle, D.A. Wilkinson, Lecithin bilayers. Density measurement and molecular interactions, Biophys. J. 23 (1978) 159–175.
[62] B.W. Koenig, K. Gawrisch, Specific volumes of unsaturated phosphatidylcholines in the liquid crystalline lamellar phase, Biochim. Biophys. Acta 1715 (2005) 65–70.

Author's personal copy

[63] D. Uhríková, P. Rybár, T. Hianik, P. Balgavý, Component volumes of unsaturated phosphatidylcholines in fluid bilayers: a densitometric study, Chem. Phys. Lipids 145 (2007) 97–105.
[64] S. Tristram-Nagle, D.J. Kim, N. Akhunzada, N. Kučerka, J.C. Mathai, J. Katsaras, M. Zeidel, J.F. Nagle, Structure and water permeability of fully hydrated diphytanoylPC, Chem. Phys. Lipids 163 (2010) 7485–7493.
[65] C. Anezo, A.H. de Vries, H.D. Holtje, D.P. Tieleman, S.-J. Marrink, Methodological issues in lipid bilayer simulations, J. Phys. Chem. B 107 (2003) 9424–9433.
[66] J.N. Sachs, H.I. Petrache, T.B. Woolf, Interpretation of small angle x-ray measurements guided by molecular dynamics simulations of lipid bilayers, Chem. Phys. Lipids 126 (2003) 211–223.
[67] R.W. Benz, F. Castro-Roman, D.J. Tobias, S.H. White, Experimental validation of molecular dynamics simulations of lipid bilayers: a new approach, Biophys. J. 88 (2005) 805–817.
[68] S.A. Pandit, S.W. Chiu, E. Jakobsson, A. Grama, H.L. Scott, Cholesterol packing around lipids with saturated and unsaturated chains: a simulation study, Langmuir 24 (2008) 6858–6865.
[69] N. Kučerka, J. Katsaras, J.F. Nagle, Comparing membrane simulations to scattering experiments: introducing the SIMtoEXP software, J. Membr. Biol. 235 (2010) 43–50.
[70] M.C. Pitman, F. Suits, A.D. Mackerell Jr., S.E. Feller, Molecular-level organization of saturated and polyunsaturated fatty acids in a phosphatidylcholine bilayer containing cholesterol, Biochemistry 43 (2004) 15318–15328.
[71] S.L. Niu, B.J. Litman, Determination of membrane cholesterol partition coefficient using a lipid vesicle-cyclodextrin binary system: effect of phospholipid acyl chain unsaturation and headgroup composition, Biophys. J. 83 (2002) 3408–3415.
[72] S.P. Soni, D.S. LoCascio, Y. Liu, J.A. Williams, R. Bittman, W. Stillwell, S.R. Wassall, Docosahexaenoic acid enhances segregation of lipids between: 2H-NMR study, Biophys. J. 95 (2008) 203–214.
[73] S.L. Veatch, S.S. Leung, R.E. Hancock, J.L. Thewalt, Fluorescent probes alter miscibility phase boundaries in ternary vesicles, J. Chem. Phys. B 111 (2007) 502–504.
[74] J. Pencer, T.T. Mills, N. Kučerka, M.-P. Nieh, J. Katsaras, Small-angle neutron scattering to detect rafts and lipid domains, in: T.J. McIntosh (Ed.), Lipid Rafts: Methods in Molecular Biology, Vol. 398 Humana Press Inc., Totowa, NJ, 2007, pp. 231–244.
[75] J. Pencer, T. Mills, V.N.P. Anghel, S. Krueger, R.M. Epand, J. Katsaras, Detection of submicron-sized raft-like domains in membranes by small-angle neutron scattering, Eur. Phys. J. E 18 (2005) 447–458.
[76] J. Pencer, V.N.P. Anghel, N. Kučerka, J. Katsaras, Scattering from laterally heterogeneous vesicles I: model independent analysis, J. Appl. Cryst. 39 (2006) 791–796.
[77] S.L. Veatch, I.V. Polozov, K. Gawrisch, S.L. Keller, Liquid domains in vesicles investigated by NMR and fluorescence microscopy, Biophys. J. 86 (2004) 2910–2922.
[78] M. Yanagisawa, M. Imai, T. Masui, S. Komura, T. Ohta, Growth dynamics of domains in ternary fluid vesicles, Biophys. J. 92 (2007) 115–125.
[79] V.N.P. Anghel, N. Kučerka, J. Pencer, J. Katsaras, Scattering from laterally heterogeneous vesicles II: the form factor, J Appl. Cryst. 40 (2007) 513–525.
[80] J. Pencer, A. Jackson, N. Kučerka, M.-P. Nieh, J. Katsaras, The influence of curvature on membrane domains, Eur. Biophys. J. 37 (2008) 665–671.
[81] G.W. Feigenson, J.T. Buboltz, Ternary phase diagram of dipalmitoyl-PC/dilauroyl-PC/cholesterol: nanoscopic domain formation driven by cholesterol, Biophys. J. 80 (2001) 2775–2788.

Author's personal copy

This page intentionally left blank